ACS Partner Journal

ACCOUNTS of materials research

pubs.acs.org/amrcda

Article

Engineering Colloidal Perovskite Nanocrystals and Devices for Efficient and Large-Area Light-Emitting Diodes

Young-Hoon Kim and Tae-Woo Lee*

Cite This: *Acc. Mater. Res.* 2023, 4, 655−667

Read Online

ACCESS | Metrics & More | Article Recommendations | Supporting Information

CONSPECTUS: Colloidal metal halide perovskite nanocrystals (PNCs) have high color purity, solution processability, high luminescence efficiency, and facile color tunability in visible wavelengths and therefore show promise as light emitters in next-generation displays. The external quantum efficiency (EQE) of PNC light-emitting diodes (LEDs) has been rapidly increased to reach 24.96% by using colloidal PNCs and 28.9% using on-substrate *in situ* synthesized PNCs. However, high operating stability and a further increase of EQE in PNC-LEDs have been impeded for three reasons: (1) Colloidal PNCs consist of ionic crystal structures in which ligands bind dynamically and therefore easily agglomerate in colloidal solution and films; (2) Long-alkyl-chain organic ligands that adhere to the PNC surface improve the photoluminescence quantum efficiency and colloidal stability of PNCs in solution but impede charge transport in PNC films and limit their electroluminescence efficiency in LEDs; (3) Unoptimized device structure and nonuniform PNC films limit the charge balance and reduce the device efficiency in PNC-LEDs.

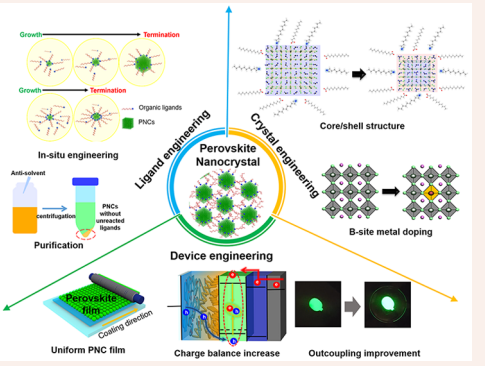

In this Account, we summarize strategies to solve the limitations in PNCs and PNC-LEDs as consequences of photoluminescence quantum efficiency in PNCs and the charge-balance factor and out-coupling factor in LEDs, which together determine the EQE of PNC-LEDs. We introduce the fundamental photophysical properties of colloidal PNCs related to effective mass of charge carriers and surface stoichiometry, requirements for PNC surface stabilization, and subsequent research strategies to demonstrate highly efficient colloidal PNCs and PNC-LEDs with high operating stability.

First, we present various ligand-engineering strategies that have been used to achieve both efficient carrier injection and radiative recombination in PNC films. *In situ* ligand engineering reduces ligand length and concentration during synthesis of colloidal PNCs, and it can achieve size-independent high color purity and high luminescent efficiency in PNCs. Postsynthesis ligand engineering such as optimized purification, replacement of organic ligands with inorganic ligands or strongly bound ligands can increase charge transport and coupling between PNC dots in films. The luminescence efficiency of PNCs and PNC-LEDs can be further increased by various postsynthesis ligand-engineering methods or by sequential treatment with different ligands. Second, we present methods to modify the crystal structure in PNCs to have alloy- or core/shell-like structure. Such crystal engineering is performed by the correlation between entropy and enthalpy in PNCs and result in increased carrier confinement (increased radiative recombination) and reduced defects (decreased nonradiative recombination). Third, we present strategies to boost the charge-balance factor and out-coupling factor in PNC-LEDs such as modification of thickness of each layer and insertion of additional interlayers, and out-coupling hemispherical lens are discussed. Finally, we present the advantages, potential, and remaining challenges to be solved to enable use of colloidal PNCs in commercialized industrial displays and solid-state lighting. We hope this Account will help its readers to grasp the progresses and perspectives of colloidal PNCs and PNC-LEDs, and that our insights will guide future research to achieve efficient PNC-LEDs that have high stability and low toxicity.

1. INTRODUCTION

Accurate reproduction of the natural color is considered the most important objective in display technology. To reproduce natural color accurately and make a display look realistic, a display device should have a wide color gamut that can fulfill the requirement of REC.2020, which is a new color standard for ultrahigh-definition television.[1] However, conventional light emitters such as organic emitters (full width at half-maximum (fwhm) ∼ 50 nm) and inorganic quantum dots (QDs) (fwhm ∼30 nm) cannot meet REC.2020. To meet it, new light emitters that have high color purity are required.[2,3]

Metal halide perovskites (MHPs) consist of three ions in an ABX_3 structure, where A is an organic ammonium (e.g., methylammonium (MA; $CH_3NH_3^+$), formamidinium (FA;

Received: March 15, 2023
Revised: June 13, 2023
Published: August 17, 2023

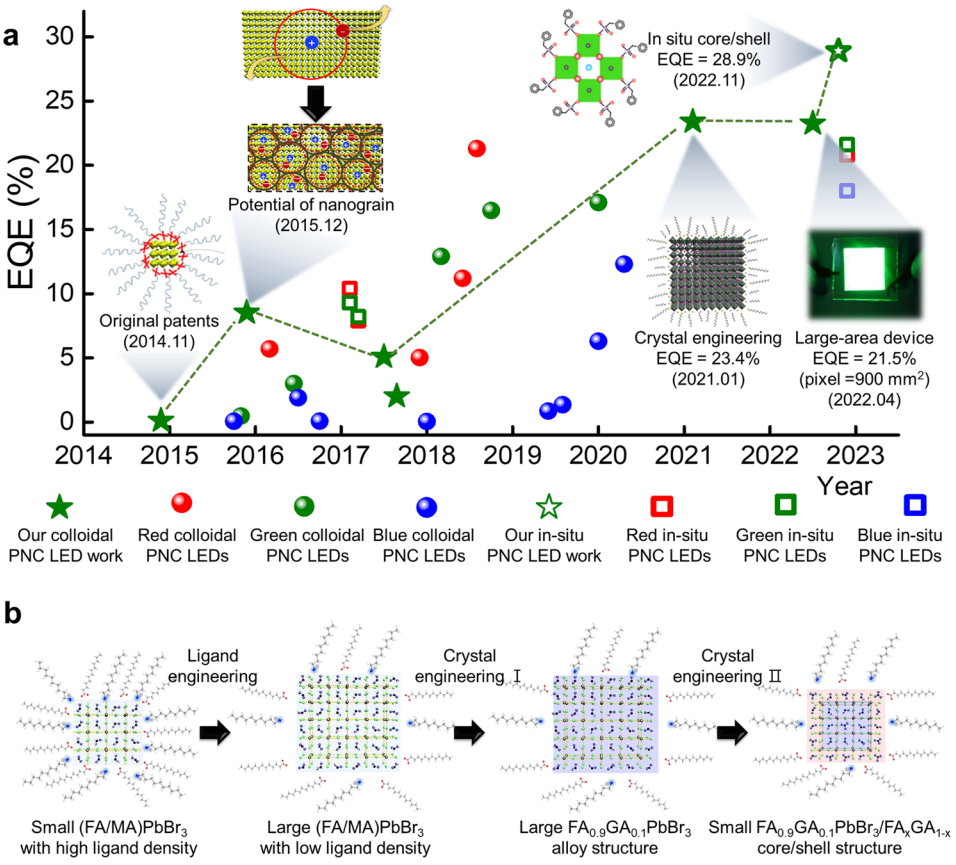

Figure 1. (a) Major development of colloidal perovskite nanocrystals (PNCs) and PNC-light-emitting diodes. Information of PNC-LEDs are summarized in Figure S1 and Table S1 in the Supporting Information. (b) Schematic illustrations describing our research strategies (ligand engineering, crystal engineering I, crystal engineering II) to increase luminescence efficiency of colloidal PNCs.

$CH(NH_2)_2^+$)) or an alkali-metal cation (e.g., Cs^+), B is a transition-metal cation (e.g., Pb^{2+}, Au^{2+}, Sn^{2+}, Mn^{2+}), and X is a halide anion (I^-, Br^-, Cl^-). They emit color that has high purity (fwhm ~20 nm) and can be tuned easily in visible wavelengths (400 to 800 nm), so they are regarded as promising light emitters to satisfy REC.2020.[4] Furthermore, MHPs have good compatibility with diverse solution processes to synthesize MHP crystals in various forms (e.g., single crystals, polycrystalline bulk films, colloidal nanocrystals).[5]

Despite these advantages, MHP light-emitting diodes (LEDs) initially achieved only faint photoluminescence (PL) intensities, and very low electroluminescence (EL) intensities at room temperature were reported in MHPs.[6,7] However, in 2015 our group demonstrated the potential of bright room-temperature MHP-LEDs[3] and high efficiency MHP-LEDs with external quantum efficiency (EQE) of 8.53% by fabricating $MAPbBr_3$ nanograins with average diameter of 99.7 nm and confining charge carriers inside the nanograins,[8] and this breakthrough stimulated interest in increasing the EL efficiency of MHP-LEDs.[9]

Furthermore, in November 2014, we applied for eight source patents including colloidal perovskite nanocrystal (PNC) particles[10] and their application in down-conversion (wavelength-converting) displays[11] and reported the high potential of PNCs as light emitters for commercialization of next-generation displays and optical sources that fulfill the Rec. 2020 standard. Colloidal PNCs confine charge carriers in small nanometer-sized crystals and prevent dissociation of excitons to free charge carriers, which occurs as a result of small exciton-binding energy.[12] Furthermore, most defects in MHP crystals have energies between those of the valence-band maximum (VBM) and conduction-band minimum (CBM) and can easily be passivated by chemical modification such as organic ligands, unlike inorganic QDs in which defects have energy levels deep in the bandgap.[13] Therefore, PNCs have high color purity light with wide color gamut in the Commission Internationale de l'Eclairage diagram, and thereby fulfill Rec 2020; they also have high photoluminescence quantum efficiency (PLQE) > 90% without use of epitaxial shells.[14] Furthermore, colloidal PNCs can be synthesized at room temperature without need for a high-vacuum system, unlike inorganic colloidal QDs, and offer reproducibility and scalability up to liter-scale or gram-scale.[15] Moreover, synthesis of PNCs in colloidal solution goes to completion, so film formation is decoupled from crystallization, and thereby enables fabrication of uniform large-area PNC films and large-area PNC-LEDs by a simple roll-to-roll process.[9] Owing to these advantages, since the report of the potential of PNC in LEDs from our group,[8,10,11] many researchers have tried to increase the luminescent efficiency (LE) of PNC-LEDs; these efforts have achieved high external quantum efficiency (EQE) of 23.4%[14] and 24.96%[16] in green emission, 21.3% in red emission,[17] and 12.3% in blue emission[18] in LEDs that used colloidal PNCs. Recently, our group achieved EQE of 28.9% in green-emitting LEDs that used PNC film that had been produced on-substrate and *in situ* by processing polycrystalline film to produce small nanograins but used a synthesis scheme directly on the substrate during

https://doi.org/10.1021/accountsmr.3c00039
Acc. Mater. Res. 2023, 4, 655−667

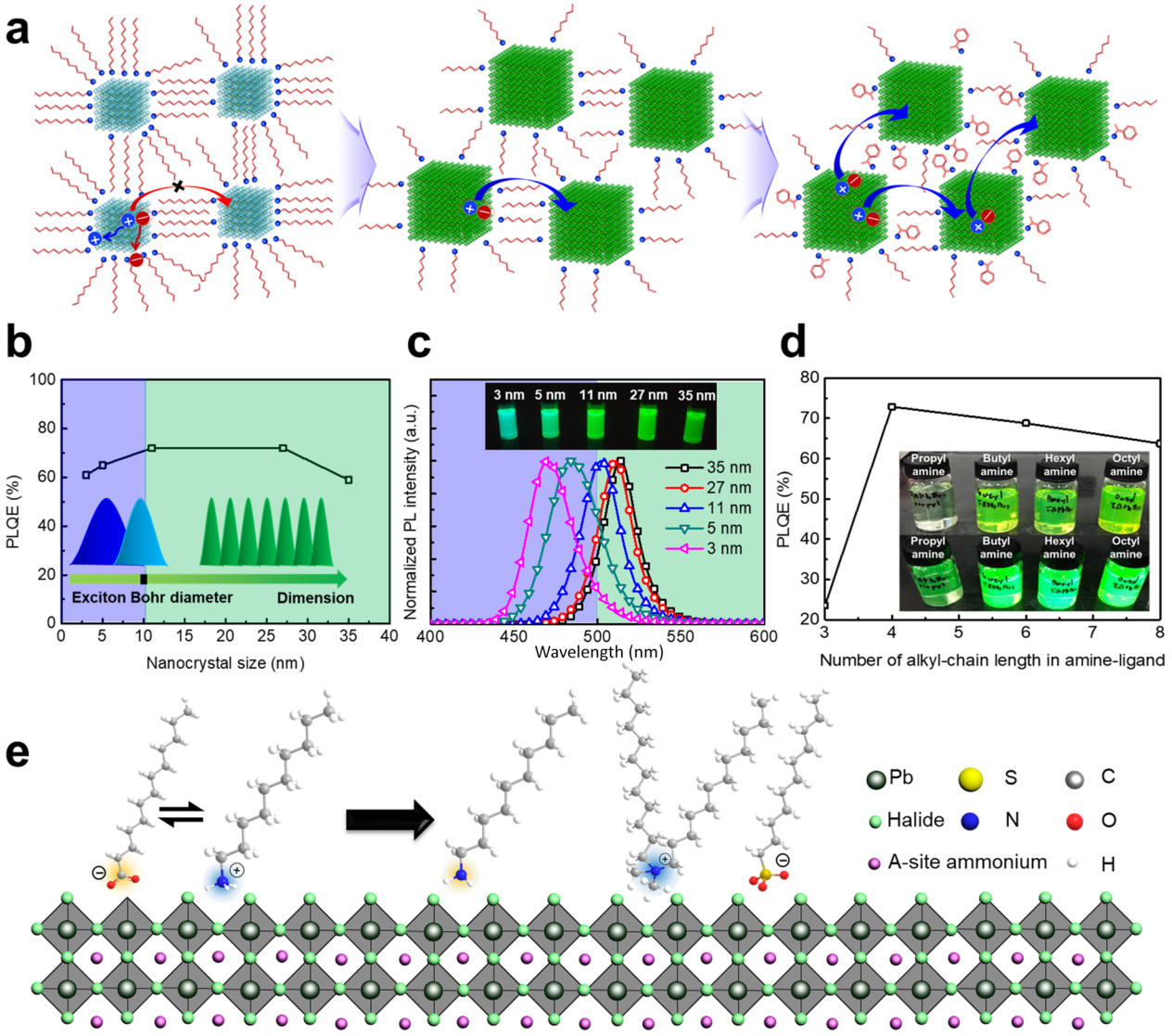

Figure 2. Schematic illustrations of nonradiative recombination and inefficient charge transport in small PNCs that have large surface-to-volume ratio (left), efficient charge transport and increased luminescence in relatively large PNCs (middle) and boosted charge transport in ligand-treated PNC films (right). (b) Photoluminescence quantum efficiency (PLQE) and (c) photoluminescence spectrum and photograph under UV light (inset) of PNCs with various nanocrystal size. Reproduced with permission from ref 12. Copyright 2017 American Chemical Society. (d) PLQE and photograph under room light (top) and UV light (bottom) (inset) of PNCs with various ligand chain length in amine ligand. Reproduced with permission from ref 29. Copyright 2017 Elsevier. (e) Schematic representation of postsynthesis ligand-exchange.

the film-formation, similarly to colloidal nanocrystal synthesis.[19]

EQE measures the device efficiency of LEDs; it is the ratio of the number of photons emitted from a device to the number of electrons injected into it, and is calculated as

$$\mathrm{EQE} = \phi_L \gamma \chi \beta$$

where ϕ_L is the quantum efficiency of luminescence (here, by PNCs), γ is the charge-balance factor, χ is the out-coupling factor, and β is the probability of production of emissive species. To maximize the EQE in PNC-LEDs, we tried to maximize each component. In this Account, we review our research progress and strategies in PNC and PNC-LEDs (Figure 1). It covers our strategies to increase the ϕ_L in PNCs by ligand engineering (section 3) and crystal engineering (section 4) and γ and χ in PNC-LEDs by device engineering (section 5). We also describe our finding that PNCs have advantages over perovskite polycrystalline bulk films for the demonstration of large-area LEDs (section 6). Finally, we will discuss current challenges and future research directions toward the development of practical display applications (section 7).

2. FUNDAMENTAL PROPERTIES OF PNCS

The optical property of an MHP depends on its components (organic ammonium or metal cation in the A site, central metal cation in the B site, halide anion in the X site) and crystal structures, because for example, in a Pb-bearing MHP the VBM is formed by the filled Pb 6*s*-halide n*p* antibonding orbitals, and the CBM is formed by unoccupied Pb 6p-halide n*s* antibonding orbitals (where n is the principal quantum number; i.e., 3 for Cl, 4 for Br, 5 for I).[20] Therefore, the emission wavelength of colloidal PNCs can be tuned by replacing components or changing the dimensionality.[21,22]

https://doi.org/10.1021/accountsmr.3c00039
Acc. Mater. Res. 2023, 4, 655−667

In perovskites, the effective mass of electrons is similar to that of holes, so the electron and hole wave functions can overlap efficiently.[22,23] Moreover PNCs have shallow traps that are mostly located on the surface and can be passivated by organic ligands.[24] Therefore, PNCs do not need an epitaxial shell and can have high PLQE and size-independent high color purity even if their size exceeds the exciton Bohr diameter D_B, unlike inorganic QDs.[23] A PNC smaller than D_B follows quantum confinement effects, so its bandgap increases and emission wavelength concomitantly blueshifts, as occurs in inorganic QDs.[12] Therefore, control of size provides another method to precisely tune their emission wavelength, but is only applicable when their size is $< D_B$.

PNCs in which A = MA or Cs, B = Pb and X = Br have size-dependent Br/Pb ratio[21] and Br/Cs ratio[25] with Br-rich stoichiometry on the surface.[21,26] The Br-rich surfaces self-passivate the undercoordinated Pb atoms and prevent the nonradiative recombination of charge carriers. Furthermore, Br-rich surfaces have larger bandgap than core crystals of ideal perovskite (ABX_3), and therefore form core/shell-like structure that facilitates radiative recombination of charge carriers.[27] PNCs with halide-poor surfaces have many trap states there, and low LE as a consequence.[28] Therefore, to achieve high PLQE and EQE in PNC-LEDs, halide defects must be passivated on the PNC surface, and this surface must be stabilized; strategies for these processes have included ligand engineering and crystal engineering.

3. LIGAND ENGINEERING

Organic ligands on the PNC surface can prevent aggregation of PNCs and thereby stabilize the colloidal PNC solution. Organic ligands can passivate the surface defects and suppress the nonradiative recombination of charge carriers, and these effects increase the ϕ_L of PNCs. However, high ligand density and the long carbon chain in these organic ligands impede charge transport and reduce the electrical coupling between PNC dots in film. On the contrary, low ligand density in the PNC surface induces imperfect surface passivation, low PLQE and instability in PNCs. Therefore, to achieve both efficient carrier injection and radiative recombination in PNC films, various ligand engineering strategies have been evaluated.

3.1. *In Situ* Engineering

When PNCs are synthesized by recrystallization in air at room temperature, their surface properties can be controlled by adjusting ligand density and ligand length. A low concentration of carboxylic acid ligand (oleic acid (OA)) during synthesis of PNCs induces an increase in PNC size to $> D_B$, which is in the regime beyond the quantum size effect, so they have high color purity and spectral wavelength that are independent of their size.[12] In contrast, a high concentration of acid ligand prevents diffusion of precursor from precursor solution to growing crystals, and thereby impedes further growth of PNCs, so they remain $< D_B$, which is within the quantum-confinement regime, so they have large surface-to-volume ratio and increased surface defects which cannot be fully passivated by organic ligands, and therefore have low PLQE (Figure 2a). Furthermore, reduction in the size of PNCs increases their surface-to-volume ratio and increases the amount of surface organic ligands that they bear; these changes degrade the charge-transport characteristics in film. PNCs that have size similar to or slightly larger than D_B maximize the PLQE and color purity, which are not affected by size and variation in size, and have efficient carrier transport in films; consequently, PNC-LEDs that use $MAPbBr_3$ PNCs have achieved EQE = 5.09% and CE = 15.5 cd/A in 2017 (Figure 2b,c).[12]

Use of short ligands (butylamine, hexylamine, and octylamine) instead of long ligands (e.g., oleylamine (OAm)) during synthesis can also slightly increase the size of PNCs and achieve facile charge transport while maintaining high PLQE (Figure 2d). However, if the ligand is too short (i.e., propylamine), it does not provide stability of PNCs in colloidal solution, permits their aggregation, and results in very low PLQE (~20%) with low concentration of PNC solution. As a consequence of *in situ* ligand length engineering, PNC-LEDs that used $FAPbBr_3$ PNCs with butylamine and OA achieved 20 times higher EL efficiency than PNC-LEDs that used octylamine and OA, which were demonstrated in 2017.[29] Furthermore, in 2018, use of short and aromatic phenethylamine during the synthesis of $CsPbBr_3$ PNCs and $CsPbI_3$ PNCs achieved PNC-LEDs that had three times higher efficiency than PNC-LEDs that used PNCs with long OA and OAm.[30]

Short aromatic ligands can be a good solution to achieve both high conductivity and high LE.[19,30,31] Aromatic ligands allow delocalization of the electron wave function and facilitate the charge transport. Phenethylamine was introduced during synthesis and phenethylammonium iodide was additionally introduced during solid-state ligand exchange, and increased the EQE of PNC-LEDs from 2.45% to 14.08% (2018).[30]

3.2. Purification

Charge injection can be increased by postsynthesis purification. Polar solvents that are used for purification of conventional inorganic QD induce redissolution of PNCs to precursor ions. Therefore, only solvents (e.g., methyl acetate, ethyl acetate) that can neither disperse nor destroy PNCs are selected for the purification.[32] After synthesis of the PNCs, these solvents are added to the as-synthesized PNC solutions and remove unreacted organic ligands, reaction solvent (e.g., octadecene), and a portion of ligands from the PNCs. Precipitated PNCs can be rewashed with intermediate solvent in a multiple-stage purification process; during these processes, ligand density on the PNCs gradually decreases and concomitantly increases charge transport characteristics in films and thereby increases current density in PNC-LEDs.[33]

Purification reduces ligand density and thus suppresses the acid−base reaction between OAm and OA ($OAm + OA \leftrightarrow OAmH^+ + OA^-$), and thereby increases the stability of PNCs in colloidal solutions.[34] However, excessive removal of organic ligands leads to insufficient passivation of surface defects, so nonradiative recombination can occur there. $CsPbBr_3$ PNCs showed maintained PLQE > 90% after two cycles of purification but it gradually decreased to <60% after the fifth cycle. PNC-LEDs that used twice-purified $CsPbBr_3$ PNCs had maximum EQE of 6.27% (2017).[33]

Appropriate use of an intermediate solvent for purification can increase the LE of PNCs. This effectiveness depends on the polarity[33] and dielectric constant[35] ε of solvents. Cosolvents of hexane and ethyl acetate with moderate polarity ($\varepsilon \approx 4.3$),[33] solvents with low dielectric constant $5 \leq \varepsilon \leq 10$ (e.g., diglyme)[35] and butyl acetate ($\varepsilon \approx 4$)[36] can effectively reduce ligand density, achieve charge transport capability in films, maintain high LE and achieve high efficiency in PNC-LEDs (EQE = 6.27% with cosolvent of hexane/ethyl acetate,

https://doi.org/10.1021/accountsmr.3c00039
Acc. Mater. Res. 2023, 4, 655−667

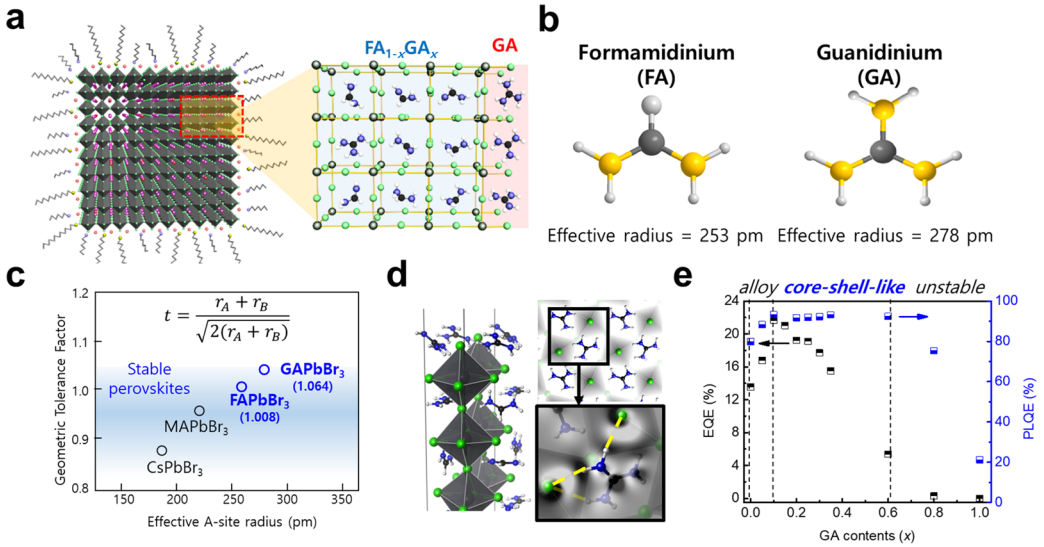

Figure 3. (a) Schematic illustrations of crystal engineered $FA_{1-x}GA_xPbBr_3$ PNC structure. Schematic illustrations of (b) formamidinium (FA) molecular structure and guanidinium (GA) molecular structure. (c) Tolerance factor of $CsPbBr_3$, $MAPbBr_3$, $FAPbBr_3$ and $GAPbBr_3$ crystals. (d) Simulated crystal structure and hydrogen bonds between the GA and Br on the $FA_{1-x}GA_xPbBr_3$ PNC surfaces in side view (left) and top view (top-right). (e) External quantum efficiency (EQE) of $FA_{1-x}GA_xPbBr_3$ PNC-LEDs and PL quantum efficiency (PLQE) of $FA_{1-x}GA_xPbBr_3$ PNCs. Reproduced with permission from ref 14. Copyright 2021 Nature Publishing Group.

2017;[33] EQE = 8.08% with diglyme, 2018;[35] EQE = 8.73% with butyl acetate, 2017[36]).

3.3. Postsynthesis Treatment

Postsynthesis treatments can efficiently passivate halide vacancies and increase charge conductivity (Figure 2e). Use of didodecyldimethylammonium bromide to replace pristine ligands (OAm and OA) increased the conductivity and EQE from ≈0.1% to ≈3% in green PNC-LEDs (2016).[37] Replacement of pristine ligands with oleylammonium iodide and aniline hydroiodide increased EQE of PNC-LEDs from 0.17% to 21.3% and 14.1% respectively (2018).[17]

Sequential treatments with two different halide sources can remove ligands more effectively than single-halide treatments, and can achieve high efficiency in PNC-LEDs.[18] Treatment of $CsPbX_3$ PNCs with isopropylammonium bromide and NaBr after purification induces formation of a bipolar shell with which the surface rich in Br^- forms a negatively charged inner shell, and the ammonium counterions form a positively charged outer shell. This bipolar shell efficiently passivates surface defects and significantly decreases electron-trap density from $n_{trap\ electron} = 1.1 \times 10^{16}$ cm^{-3} and hole-trap density from $n_{trap\text{-}hole} = 1.1 \times 10^{16}$ cm^{-3} in control PNCs to $n_{trap\text{-}electron} = 0.03 \times 10^{16}$ cm^{-3} and $n_{trap\text{-}hole} = 0.1 \times 10^{16}$ cm^{-3} in PNCs with bipolar shells.[18] The bipolar shell also protects PNCs from external quenching moieties and provides excellent stability with high PLQE > 90% in $CsPbX_3$ PNCs.

$CsPbX_3$ PNCs with a bipolar shell do not have long-alkyl-chain ligands and form dots separated by 4.2 nm, which is shorter than in control $CsPbX_3$ PNCs that have normal organic ligands. The absence of insulating ligands on the surfaces and short distance between dots enable efficient coupling between PNC dots with high electron mobility $\mu_e = 0.02$ cm^2 V^{-1} s^{-1} and hole mobility $\mu_h = 0.01$ cm^2 V^{-1} s^{-1}. Therefore, $CsPbX_3$ PNCs that have the bipolar shell achieved EQE = 12.3% in blue-emitting PNC-LEDs and EQE = 22% in red-emitting PNC-LEDs (2020).[18]

Postsynthesis treatment using hydrobromic acid (HBr) followed by two amine ligands (didodecylamine (DDDAM), phenethylamine (PEA))[38] passivated the defects in small (∼4 nm) $CsPbBr_3$ QDs. HBr first removes imperfect octahedra and excessive organic ligands from the QD surface. Then DDDAM and PEA passivate the residual uncoordinated sites and achieved near-unity PLQE (∼97%) in $CsPbBr_3$ QDs and high EQE (∼4.7%) in LEDs at pure-blue emission (wavelength ∼470 nm) (2021).[38]

3.4. Inorganic Ligands

Inorganic ions can efficiently passivate halide vacancies on the PNC surface and are smaller than long-chain organic ligands and thus enable coupling between dots in PNC films. Partial replacement of organic ligands with metal bromide salts ($ZnBr_2$, $MnBr_2$, $GaBr_2$, $InBr_2$) passivates defects, increases conductivity, and achieved high PLQE of 74% in $CsPbBr_3$ PNCs and EQE of 16.48% in PNC-LEDs (2018).[39] Thionyl halides ($SOCl_2$, $SOBr_2$ or a mixture thereof) can also passivate surface defects and prevent critical degradation of PNCs upon multiple purification.[40] Additional coating of thionyl halides on synthesized $CsPb(Cl/Br)_3$ PNCs maintained high PLQE > 80% even after four sequential purifications, whereas control PNCs without additional thionyl halides showed reduced PLQE < 40% after four purification cycles. Treatment with KI reduced trap density from $n_{trap\text{-}electron} = 5.5 \times 10^{15}$ cm^{-3} and $n_{trap\text{-}hole} = 4.35 \times 10^{15}$ cm^{-3} in control PNCs to $n_{trap\text{-}electron} = 1.05 \times 10^{15}$ cm^{-3} and $n_{trap\text{-}hole} = 1.4 \times 10^{15}$ cm^{-3} in treated PNCs; these changes yielded high EQE = 23% and excellent operating stability of 10 h at luminance of 200 cd m^{-2} (2021).[41]

Pseudohalogens such as cyanogen and cyanide ions have properties that resemble those of true halogens and can passivate halide vacancies on PNC surfaces. *n*-Dodecylammonium thiocyanate ($C_{12}H_{25}NH_3SCN$) is an organic thiocyanate with a long carbon chain, and has high solubility in nonpolar solvent (>100 mg in toluene). The concentration of *n*-dodecylammonium thiocyanate for the treatment can be easily

https://doi.org/10.1021/accountsmr.3c00039
Acc. Mater. Res. 2023, 4, 655−667

controlled.[42] *n*-Dodecylammonium thiocyanate fills the halide vacancy, donates electrons to the undercoordinated Pb atoms on the PNC surfaces, and passivates Cl^- defects in $CsPb(Br_xCl_{1-x})_3$ PNCs; this change yielded near-unity PLQE (~100%) and high EQE of 6.3% in blue emission (2020).[42]

PNCs can be imbedded in halide perovskite $(PEA_2Cs_{n-1}Pb_n(I_{0.6}Br_{0.4})_{3n+1}$, where PEA is phenylethylene ammonium) matrix.[43] Before the formation of PNC-in-matrix films, $CsPbI_3$ PNCs were protected by formation of a bipolar shell by sequential treatment with isopropylammonium iodide and KI. This shell protects $CsPbI_3$ PNCs from dissolution in polar solution that contains perovskite precursors. During spin coating of $CsPbI_3$ PNC/perovskite precursor solution, low-dimensional perovskite matrix crystallizes on the PNC surface and forms PNC-in-matrix heteroepitaxial structure, in which charge carriers are funneled into PNCs with smaller bandgap than low-dimensional matrix $(PEA_2Cs_{n-1}Pb_n(I_{0.6}Br_{0.4})_{3n+1})$ and then radiatively recombine. Under a high electric field, charge carriers are partially delocalized into the matrix, release a large population of charge carriers, and suppress nonradiative Auger recombination in small PNCs; this process yielded PNC-LEDs that have a high EQE = 18%, and excellent operating stability of 2100 h at initial luminance of 100 cd m^{-2} (2021).[43]

Weak and dynamic bonding between OAm/OA ligands and PNC surfaces[34,44] and acid−base equilibrium by proton exchange between OAm and OA[25,44] ($OAm + OA \leftrightarrow OAmH^+ + OA^-$) induce detachment of ligands from PNC surfaces, imperfect surface passivation, and instability in PNCs. Therefore, replacing the ligands of OAm, OA, or both with new ligands that bind more strongly than they do to the PNC surface constrained those reactions and increased the stability of PNCs in solution (Figure 2e). The detailed methods to replace OAm, OA, or both with new ligands are described in section 3.1 of the Supporting Information.

4. CRYSTAL ENGINEERING

We designed crystal-engineering strategies that confine charge carriers inside smaller PNCs and passivate surface defects, and that can simultaneously boost radiative recombination and suppress nonradiative recombination (Figure 3a) in 2021.[14] We doped guaninidium (GA^+, $(NH_2)_3C^+$) into $FAPbBr_3$ PNCs during synthesis. Compared to FA, GA has a larger ionic radius, which is beyond the tolerance factor of the lead-bromide perovskite structure and cannot form a stable perovskite structure (ABX_3) (Figure 3b,c). However, a small concentration of GA ([GA] ≤ 12.5 mol %) can be dissolved into the $FAPbBr_3$ structure due to entropy stabilization (i.e., mixture of GA and FA). This result indicates that GA can be uniformly doped into perovskite crystals up to [GA] = 12.5% to generate uniformly GA-doped $FAPbBr_3$ PNCs. However, at [GA] > 12.5 mol %, excess GA cannot enter the crystals and tends to move to the surface of the PNCs, where it forms a core/shell-like structure.[14] This GA behavior in $FAPbBr_3$ PNCs according to [GA] has been verified by DFT calculation of formation energy considering internal energy and configurational entropic stabilization energy, photoluminescence spectrum experiments and experimental X-ray diffraction patterns.[14]

GA has one more amino group than does FA, so inside $FAPbBr_3$ PNCs doped with [GA] = 10 mol %, this group stabilizes crystals as a result of the entropic stabilization energy and of the increasing number of hydrogen bonds with undercoordinated surface Br^- (Figure 3d). These stabilization effects reduce the defect density from 4.93×10^{12} cm^{-3} to 3.10×10^{12} cm^{-3}, and increase PL lifetime from ~88 to 113 ns and PLQE from 79.7% to 93.3% (Figure 3e).[14] Furthermore, GA-doped $FAPbBr_3$ PNCs had stabilized crystal structure, and thus showed increased thermal stability, photostability, exciton binding energy and critical bias in magnetoresistance.[14]

At [GA] > 10 mol %, extra GA segregates to the PNC surface because surface $PbBr_6$ octahedra cages are broken, so large GA can favorably fit into the surface sites. Surface GA can interact with surface Br^- and passivate the surface defects. This effect stabilizes the PNC surface internally and reduces its reactivity toward external agents; as a result, surface-located GA increases the surface-to-volume ratio by decreasing the size of the PNC. Therefore, charge carriers are more confined and radiatively recombined in small (~8.3 nm) and monodisperse PNCs, whereas large surface sites are passivated by extra GAs that become located on the broken $PbBr_6$ octahedra cages. GA-doped $FAPbBr_3$ PNCs maintain a high PLQE = 92.4% up to [GA] = 60%. In addition, GA-doped $FAPbBr_3$ PNCs are synthesized in a toluene-based solution through ligand-assisted reprecipitation methods and made into a thin film without complicated purification processes using antisolvents, so that a high PLQE (92.45%) can be maintained in the film. We verified experimentally that GA has similar effects on $MAPbBr_3$ PNCs.[14]

GA-doped PNCs with different [GA] concentrations have been applied in PNC-LEDs. As [GA] was increased to 10%, the LE increased in PNC light emitters, so PNC-LEDs showed an increased current efficiency from 61.3 to 95.7 cd/A and EQE from 13.5% to 21.6%. As [GA] exceeded 10%, PNC-LEDs showed gradually decreased device EQE to 5.37% at [GA] = 60%, whereas at $10 \le [GA] \le 60\%$, PNCs maintained high $92 \le PLQE \le 93\%$ (Figure 3e). We hypothesize that the different trends in PLQE of PNCs and EQE of PNC-LEDs at $10 \le [GA] \le 60\%$ occurs because as PNC size decreases, those with high [GA] have increased ratio of insulating organic ligands to perovskite crystal in PNC films and that these ligands impede efficient charge transport and thereby reduce the device efficiency in PNC-LEDs. Therefore, we conclude that $10 \le [GA] \le 12.5\%$ is the optimal [GA] to suppress defects (both bulk and surface) and maintain the original dimensionality and composition in crystals, and that this [GA] can simultaneously increase the radiative recombination of the colloidal PNCs and EQE of the PNC-LEDs.[14] B-site doping of PNCs with metal ions such as Sr^{2+} and Zn^{2+} can also increase both PLQE of PNCs and EQE of PNC-LEDs.[39,45]

5. DEVICE ENGINEERING

5.1. Fabrication of Uniform PNC Films

To achieve a high EL efficiency in PNC-LEDs, the PNC films must be uniform. However, PNCs easily aggregate in highly concentrated solution[46] or during film fabrication,[12] so PNC films on a conventional poly(3,4-ethylenedioxythiophene): poly(styrenesulfonate) (PEDOT:PSS) hole-injection layer are inhomogeneous, with particle aggregates and many pinholes.[46] The aggregates enable the development of electrical shunt paths, which yield leakage current in PNC-LEDs. We fabricated uniform, pinhole-free PNC films by modifying the underlayer and depositing a dilute PNC solution multiple times.[12] We added perfluorinated ionomer (PFI) to PEDOT:PSS in a solution and then spin coated the composite solution on the film. Surface energy is lower in PFI (~23 mN/

https://doi.org/10.1021/accountsmr.3c00039
Acc. Mater. Res. 2023, 4, 655−667

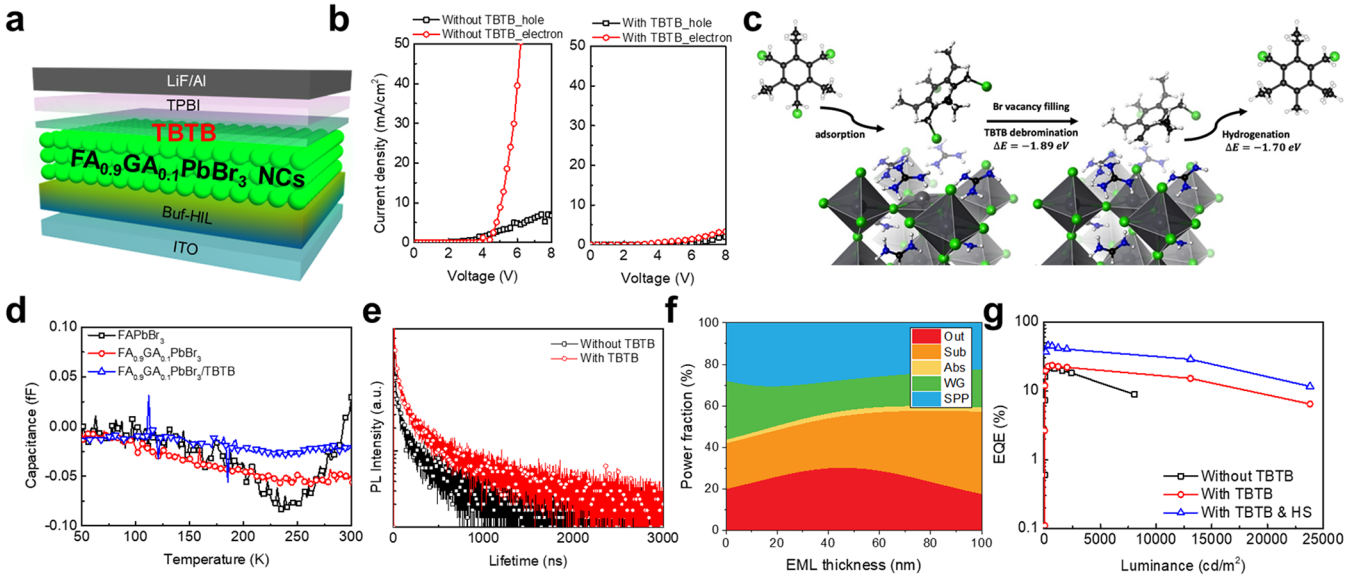

Figure 4. (a) Device structure of $FA_{0.9}GA_{0.1}PbBr_3$ PNC-LEDs with TBTB interlayers. (b) Electron-current densities in electron-only devices (left) and hole-current densities in hole-only devices (right) without and with TBTB interlayers. (c) Simulated mechanism of halide vacancy passivation by TBTB molecules on $FA_{0.9}GA_{0.1}PbBr_3$ PNC surface. (d) Deep-level transient spectroscopy data of PNC-LEDs based on $FA_{1-x}GA_xPbBr_3$ PNC without and with TBTB interlayer. (e) PL lifetime of $FA_{0.9}GA_{0.1}PbBr_3$ PNC films without and with TBTB interlayer. (f) Optical simulation of PNC-LEDs and simulated power fraction of each optical mode as a function of PNC (emitting layer, EML) thickness (Out: out-coupling mode, Sub: substrate mode, Abs: absorption mode, WG: waveguide mode, SPP: surface plasmon mode). (g) External quantum efficiency of PNC-LEDs that use $FA_{0.9}GA_{0.1}PbBr_3$ PNCs without and with TBTB interlayers. Reproduced with permission from ref 14. Copyright 2021 Nature Publishing Group.

m) than in PEDOT:PSS (~38 mN/m), so during spin coating, PFI tends to locate on the PEDOT:PSS as a result of self-organization[3] A PFI-rich surface is more hydrophobic than PEDOT:PSS, and therefore prevents aggregation of PNCs during their multiple coating steps and yields highly uniform PNC films (root-mean-squared roughness = 3.46 nm). Furthermore, Buf-HIL can increase charge balance and charge confinement in PNC-LEDs because Buf-HIL has high ionization energy >5.9 eV and can facilitate hole injection into PNC emitting layer. In addition, to maintain the high PLQE of PNCs in the thin film, we used PNCs synthesized by the ligand assisted reprecipitation (LARP) method, which does not necessarily require multiple complicated purification processes using antisolvents.[9,12,14] The PFI-rich top surface has a high work function of 5.95 eV and also facilitates hole injection from the ITO electrode to the perovskite emitting layer. Furthermore, the PFI-rich top surface can prevent exciton quenching at the interface, and thereby provide high EL efficiency in PNC-LEDs (EQE = 5.09%, CE = 15.5 cd/A for $MAPbBr_3$ PNC-LEDs) (2017).[12] Besides, PFI thin layer on top of poly(N,N′-bis(4-butylphenyl)-N,N′-bis(phenyl)-benzidine) (poly-TPD) can prevent exciton quenching and increase hole injection efficiency.[47] A polyethylene imine (PEI) underlayer was also used to fabricate uniform PNC films and achieved EQE = 6.3%, CE = 3.4 cd/A in red-emitting PNC-LEDs with inverted structure (2016).[48] The specific methods to fabricate the uniform PNC film and cover the pinholes in the PNC films from other researchers are described in section 3.2 of the Supporting Information.

5.2. Charge-Balance Increase

EQE in PNC-LEDs is also strongly affected by charge balance γ. To improve it, we applied a thin insulating organic interlayer of 1,3,5-tris(bromomethyl)-2,4,6-triethylbenzene (TBTB) on GA-doped $FAPbBr_3$ PNC films (Figure 4a).[14] The insulating TBTB interlayers on the PNC films retard electron injection into PNC films and improve the γ in PNC-LEDs. This effect was confirmed by comparing electron-current density in electron-only devices to hole-current density in hole-only devices (Figure 4b) and by measuring capacitance−voltage characteristics in PNC-LEDs. The TBTB molecule also donates bromine into residual bromide vacancies in PNC films, and this defect-healing effect reduces the defect density from 3.1×10^{12} cm^{-3} to 1.7×10^{12} cm^{-3} (Figure 4c−e). These combined effects of TBTB achieved current efficiency = 108 $cd \cdot A^{-1}$ and EQE = 23.4% in PNC-LEDs with great reproducibility (2021).[14] In inverted structure PNC-LEDs, PEI interlayer reduces the workfunction of underlying ZnO layer,[48] and $ZnCl_2$ interlayer in the middle of PNC layers slows down the transport of charge carriers,[49] both of which were used to increase the electron injection and improve charge balance in devices. Furthermore, all-inorganic electron transport layer such as ZnO/ZnS core/shell nanocrystals were used to increase the electron injection and improve charge balance in devices.[50]

5.3. Increasing Outcoupling

To maximize the EL efficiency of PNC-LEDs, the out-coupling factor χ of generated light should be increased. Optimization of the thickness of each organic or perovskite film is one way to increase this efficiency. We performed optical simulation and calculated χ in our devices as a function of PNC film thickness x [glass/indium tin oxide (70 nm)/PEDOT:PSS: PFI (x nm)/PNC emission layer (EML) (50 nm)/TBTB (5 nm)/ 2,2′,2″-(1,3,5-Benzinetriyl)-tris(1-phenyl-1-H-benzimidazole) (TPBI) (50 nm)/LiF (1 nm)/Al (100 nm)] (Figure 4f).[14] To isolate χ in the simulation, the internal quantum efficiency of PNC films was set to 100%, and the absorption loss of the EML was set to be negligible in the emission spectrum. The emission zone was set to be located at the center of EML as we optimized the

https://doi.org/10.1021/accountsmr.3c00039
Acc. Mater. Res. 2023, 4, 655−667

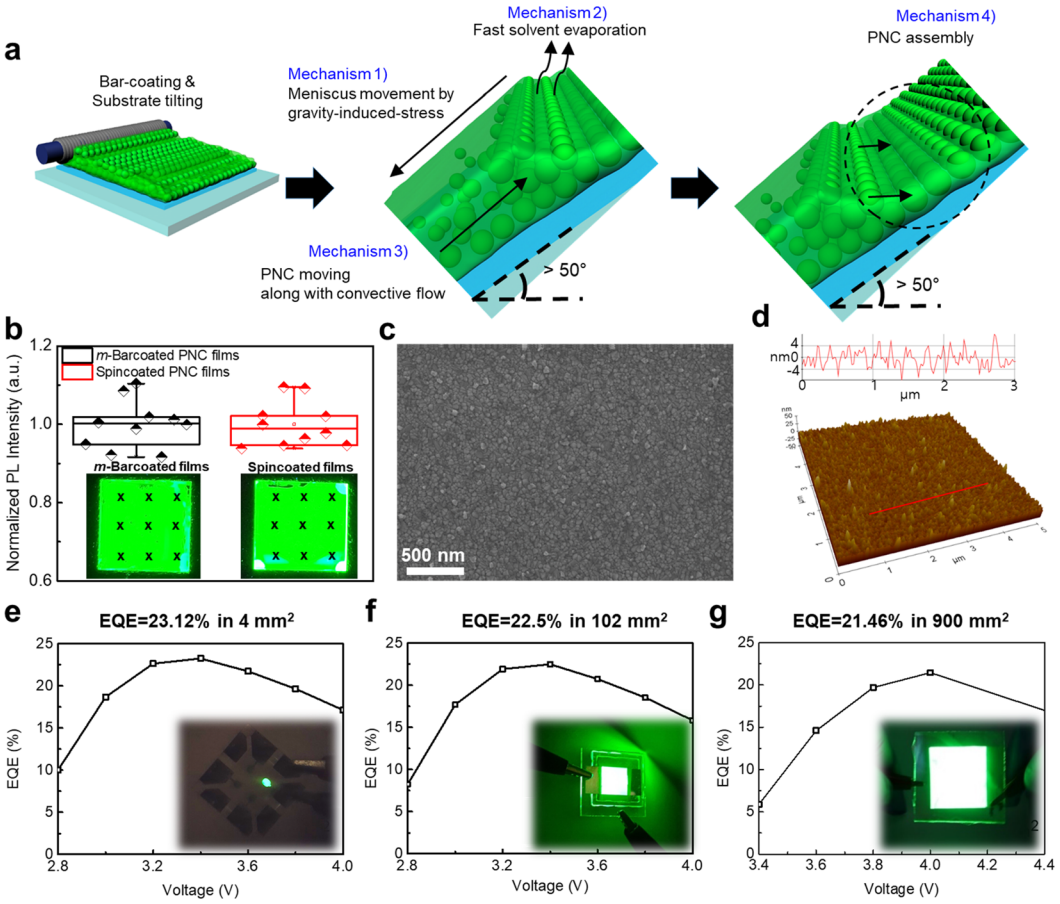

Figure 5. (a) Schematic illustrations of fabrication of uniform PNC films by *m*-barcoating with following mechanisms: 1) downward flow of colloidal solution upon the tilting of substrate, 2) fast evaporation of residual solvent, 3) PNC moving along with convective flow, and 4) assembly of PNCs ahead of the moving meniscus. (b) Normalized PL intensity of *m*-barcoated and spin-coated PNC films measured at × (insets). (c) Scanning electron microscope (SEM) image and (d) atomic force microscopy (AFM) image (bottom) and cross-sectional roughness (top) of *m*-barcoated PNC films. External quantum efficiency and photograph of operating devices (inset) of PNC-LEDs with pixel area of (e) 4 mm^2, (f) 102 mm^2 and (g) 900 mm^2. Reproduced with permission from ref 9. Copyright 2022 Nature Publishing Group.

charge balance, guided by the results of the experiments with the electron-only and hole-only devices.[14] The simulation indicated that PNC-LEDs can achieve EQE = 30.2% when the EML thickness is ∼40 nm. Guided by this result, we fabricated PNC films with a thickness of 30−40 nm and achieved EQE = 23.4% in PNC-LEDs that used them (Figure 4g).[14] The difference between the 30.2% (theoretical EQE) and the 23.4% (EQE achieved in our devices) may occur because the PNCs have PLQE < 100%. We increased the EQE of PNC-LEDs to 45.5% by placing a hemispherical lens under the transparent glass substrate to boost χ in the devices (2021; Figure 4g).

χ in PNC-LEDs can be increased by controlling the direction of transition-dipole-moment (TDM) orientation in PNCs.[16] Control of the TDM orientation in PNCs has been achieved by self-assembly of anisotropic nanocrystal superlattices (length = 11 nm, thickness = 4 nm, aspect ratio = 2.75).[16] $FA_{0.5}MA_{0.5}PbBr_3$ anisotropic nanocrystal superlattices can be stacked to have a thickness of ∼32 nm (average 6−8 layers) and a lateral dimension of >300 nm by shear-induced ordering during spin coating. Anisotropic nanocrystal superlattices showed preferentially horizontal TDM orientation with an increased horizontal dipole ratio up to 0.75. As a result, anisotropic nanocrystal superlattices increased theoretical EQE to ∼32% and achieved high EQE = 24.96% in green-emitting PNC-LEDs (2022).[16] Lithium bis(trifluoromethanesulfonyl)-imide on top of $CsPbBr_3$ PNCs also controls TDM orientation and increases χ in PNC-LEDs.[51]

6. TOWARD COMMERCIALIZATION

By using various strategies, we achieved EQE of 23.4% in LEDs that used colloidal PNCs[14] and EQE of 28.9% in LEDs that used PNC film which had been directly synthesized *in situ* on substrates.[19] We also tried to demonstrate a large-area device to provide a promising approach toward the development of large-scale displays and solid-state lighting devices that use perovskite light-emitters. Perovskite polycrystalline bulk films crystallize during film formation; as a consequence, uniform polycrystalline thin films (thickness <50 nm) in a large-area cannot be easily fabricated, and this difficulty complicates the transfer of the process to scalable manufacturing for mass production.[52] However, colloidal PNCs are precrystallized and not affected by the film-formation process, so uniform PNC thin films can be produced without severe effects by processing environment and conditions.[9] Therefore, we used modified bar-coating (*m*-barcoating) in which tilting of the substrate following the barcoating of PNC solution induces downward flow of colloidal solution, coupled with fast evaporation of residual solvent and concomitant assembly of PNCs ahead of the moving meniscus by the attractive capillary forces between the moving meniscus and the under layer. PNC films

https://doi.org/10.1021/accountsmr.3c00039
Acc. Mater. Res. 2023, 4, 655−667

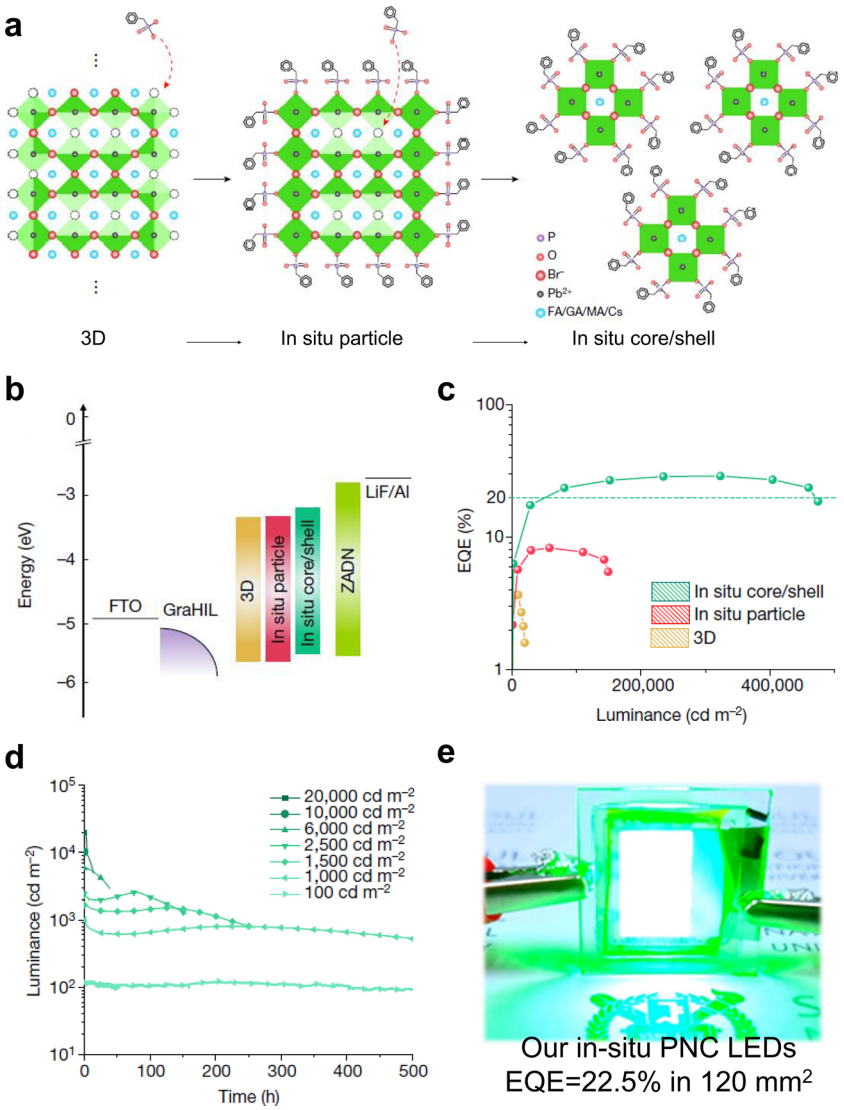

Figure 6. (a) Schematic illustrations of structures of 3D (left), *in situ* particle (middle) and *in situ* core/shell PNCs (right) by BPA treatment. (b) Energy diagram and (c) EQE versus luminance characteristics of PNC LEDs that use 3D, *in situ* particles or *in situ* core/shell PNCs. (d) Initial-brightness-dependent luminance versus time characteristics of LEDs that use *in situ* core/shell PNCs. (e) Photograph of operating large-area LEDs that use PNCs formed *in situ* by exploiting BPA treatment. Reproduced with permission from ref 19. Copyright 2022 Nature Publishing Group.

fabricated by *m*-barcoating with tilting angle ≥50° showed uniform film morphology and were used to fabricate large-area PNC-LEDs (Figure 5a–d). If large-area films have nonuniform film morphology and impurities or defects, these nonuniformities can lead to current concentration and concomitant local heating, which can degrade LED performance such as emission wavelength, device efficiency, and device stability. Our PNC thin films have uniform morphology and thus their EL efficiencies were only weakly affected by pixel dimension (23.26% for 4 mm^2, 22.5% for 102 mm^2, 21.46% for 900 mm^2) (Figure 5e–g).[9] The EQE of large-area PeLEDs can be calculated by measuring EL spectra through spectrometer and assuming Lambertian emission profile[52] or by directly measuring EL spectra using an integrating sphere connected to the spectrometer.[53] In particular, when measuring the EQE of large-area PeLEDs using a Minolta Cs2000 spectroradiometer, it is possible to control various dimensions of the PeLED by selecting the measuring angle in the spectroradiometer.[9]

Recently, we synthesized core/shell PNC-LEDs *in situ* on substrates;[19] these devices overcame the limited EL efficiency and low operating stability in colloidal PNC-LEDs. Core/shell PNCs can be formed *in situ* on substrates by exploiting the reaction between benzylphosphonic acid (BPA) and 3D ($(FA_{0.7}MA_{0.1}GA_{0.2})_{0.87}Cs_{0.13}PbBr_3$) perovskites in a precursor solution. BPA splits large perovskite crystals to small PNCs (average size ∼10 nm, increase of charge confinement) and passivates the defect sites (decrease of nonradiative recombination), and thereby forms BPA/3D core/shell PNCs (Figure 6a). Moreover, core/shell PNCs that are formed *in situ* on substrates (*in situ* core/shell PNCs) maintain a high charge transport property because insulating organic ligands such as OA and OAm are not used. By using these *in situ* core/shell PNCs, we achieved maximum brightness of 470,000 cd m^{-2}, maximum EQE of 28.9%, current efficiency of 151 cd A^{-1} and half-lifetime of 520 h at 1000 cd m^{-2} (estimated half-lifetime >30,000 h at 100 cd m^{-2}) in PNC-LEDs (Figure 6b–d) (2022). These operating stability in core/shell PNC-LEDs is superior to those of previously reported literature (half-lifetime

https://doi.org/10.1021/accountsmr.3c00039
Acc. Mater. Res. 2023, 4, 655–667

of 4806 h at 100 cd m^{-2} in perovskite polycrystalline bulk film based LEDs, half-lifetime of 180 min at ~1000 cd m^{-2} in PNC-LEDs).[54] These PNC-LEDs that use *in situ* core−shell PNC also showed high EQE of 22.5% in a large area (pixel dimension = 120 mm^2) (Figure 6e). *In situ* core/shell PNCs were used to demonstrate highly efficient red-emitting, green-emitting, and blue-emitting LEDs (EQE of 20.8%, 21.6% and 18% with a pixel area of 9 mm^2, respectively) (2022).[55] Furthermore, perovskite/perovskite core/shell structure PNCs can increase both PLQE and EQE in PNC-LEDs.[56,57]

7. CONCLUSION AND PERSPECTIVES

This Account reviews the progress of PNCs and PNC-LEDs from our own work and perspective. We have explained our research strategies by coupling with factors that determine the EQE of PNC-LEDs (LE, ϕ_L in PNCs, charge-balance factor γ and out-coupling factor χ in LEDs). Highly luminescent PNCs with high conductivity in the film can be achieved by various ligand-engineering and crystal-engineering methods. Our group and others have devoted efforts to find new ligands, crystal structures, and processing conditions to achieve near-unity PLQE in both film states and solution states. Efficient charge balance and out-coupling in PNC-LEDs can be realized by introducing uniform PNC films, additional charge-injecting or charge-impeding interlayer, optical simulation, and out-coupling hemispherical lens. By using these strategies, our group achieved a high EQE = 23.4% and current efficiency = 108 cd/A (EQE = 45.5%, CE = 205 cd/A with a light out-coupling hemispherical lens) in green-emitting PNC-LEDs. We have also demonstrated efficient large-area PNC-LEDs with pixel dimensions up to 900 mm^2. Furthermore, *in situ* core/shell PNCs can confine charge carriers, passivate defects, and facilitate charge transport in films, and as a result obtain ultrahigh EQE = 28.9%, CE = 151 cd A^{-1} and half-lifetime of 520 h at 1,000 cd m^{-2} in PNC-LEDs.

These significant achievements in efficiency and large-area devices show the potential of PNCs and PNC-LEDs for use in large-scale industrial displays and solid-state lighting. However, for the commercialization of PNC-LEDs, some remaining challenges must be overcome:

(1) Device stability. In both PNCs and PNC-LEDs, the stability is still inferior to the state-of-the-art inorganic quantum dot (QD) LEDs and to the requirements for industrial applications (retain ≥95% of initial luminance for >5,000 h).[58] This low operating stability in PNC-LEDs is mainly a result of ion migration upon application of an electric field, because PNCs consist of ionic crystal structures with dynamic bonding of ligands. Prevention of ion migration and increase in device stability require: (i) formation of PNCs that have core/shell structure[59] or gradient-alloy structure[60] by developing epitaxial shells, and (ii) invention of new organic or inorganic ligands that do not have such dynamic behaviors.[31] As our group recently reported, *in situ* core/shell PNCs can achieve high device stability because of suppression of charge accumulation and increased charge balance and transport owing to the absence of insulating ligand.[19] Furthermore, further efforts to develop optimized *in situ* core/shell PNCs, and dopant-host systems such as PNC-in-organic matrix could suppress the ion migration and induce efficient charge confinement in the PNCs.

(2) Toxicity of Pb. Toxic Pb ions in PNCs can be replaced with other metal cations such as Sn^{2+}, Bi^{3+}, Sb^{3+} and Ge^{2+}.[61−63] However, these metal ions oxidize easily (*e.g.*, Sn^{2+} to Sn^{4+}, Ge^{2+} to Ge^{4+}) or have instable crystal structure; these characteristics result in low PLQE in PNCs and low EQE in PNC-LEDs. Recently, double MHPs which include two different metal cations (*e.g.*, Bi^{3+} with Ag^+ or Sb^{3+} with Ag^+), have been reported to have stable crystal structure and high PLQE. However, their EQEs in LED devices are still inferior to state-of-the-art PNC-LEDs that use Pb, and to state-of-the-art inorganic QD-LEDs. Therefore, attention should be devoted to increasing both the EQE and the operating stability of PNC-LEDs that use Pb-free PNCs.

(3) Blue emission. Blue-emission PNC-LEDs still have low EQE (12.3% from $CsPbBr_3$ PNC-LEDs,[64] 18% from on-substrate in situ synthesized $CsPbBr_3$ PNC-LEDs[55]) compared to green-emission PNC-LEDs (23.4% from colloidal (FA/GA)$PbBr_3$ PNC-LEDs,[14] 28.9% from in situ synthesized (FA/MA/GA/Cs)$PbBr_3$ PNCs[19]) and red-emission PNC-LEDs (21.3% from $CsPb(Br/I)_3$ colloidal PNC-LEDs[17]). Two main strategies have been used to induce blue emission from PNCs: (i) incorporation of Cl^- and (ii) decrease in dimensionality of crystals or shape of PNCs to induce quantum confinement effect. Mixing Cl^- with Br^- could induce halide segregation and concomitant collapse of crystal structure. Furthermore, the volatility of Cl^- could reduce the stability of PNCs. Dimensionality of the crystal inside the PNCs can be reduced by incorporating a bulky organic cation in the A-site, but this anion has an insulating nature that can destabilize the PNCs in colloidal solution and impede charge transport in PNC films. Anisotropic PNCs such as two-dimensional perovskite nanoplatelets can emit blue light by the quantum confinement effect in an out-of-plane direction but have numerous defects due to their large surface-to-volume ratio and aspect ratio. Therefore, demonstration of highly efficient and stable blue-emitting PNC-LEDs requires further research on stabilizing PNCs that contain Cl^-, suppressing halide segregation in mixed-halide PNCs, and obtaining low-dimensional PNCs with low defect densities in either crystal structure or shape. Furthermore, demonstration of blue-emission PNC LEDs requires further intensive efforts on *in situ* core/shell PNC-LEDs, because the size of these PNCs can be controlled below D_B by tuning of reaction time between ligands and perovskite[19] or ligand concentration.[55]

We expect that this Account can help the readers to grasp the progress and perspectives of colloidal PNCs and PNC-LEDs. We also hope that future research efforts and directions can overcome the current limitation of PNCs and contribute to commercialization of PNCs and PNC-LEDs in industrial displays and solid-state lighting.

■ ASSOCIATED CONTENT

Supporting Information

The Supporting Information is available free of charge at https://pubs.acs.org/doi/10.1021/accountsmr.3c00039.

Progress of colloidal perovskite nanocrystals (PNCs) and PNC-light-emitting diodes; summary of PNC-LEDs; supplemental content and references (PDF)

https://doi.org/10.1021/accountsmr.3c00039
Acc. Mater. Res. 2023, 4, 655−667

AUTHOR INFORMATION

Corresponding Author

Tae-Woo Lee − *Department of Materials Science and Engineering, School of Chemical and Biological Engineering, Institute of Engineering Research, Research Institute of Advanced Materials, Soft Foundry, Seoul National University, Seoul 08826, Republic of Korea; SN Display Co. Ltd., Seoul 08826, Republic of Korea;* orcid.org/0000-0002-6449-6725; Email: twlees@snu.ac.kr

Author

Young-Hoon Kim − *Department of Energy Engineering, Hanyang University, Seoul 04763, Republic of Korea*

Complete contact information is available at: https://pubs.acs.org/10.1021/accountsmr.3c00039

Author Contributions

Both authors contributed to writing of the manuscript and have approved its final version.

Notes

The authors declare no competing financial interest.

Biographies

Young-Hoon Kim is an assistant professor in Department of Energy Engineering at Hanyang University. He received his Ph.D. at the Pohang University of Science and Technology (POSTECH), Korea in Korea. He worked at the Seoul National University, Korea (2016-2019), and at the National Renewable Energy Laboratory (NREL), USA (2019-2021) as a postdoctoral researcher. His research focuses on synthesis of organic−inorganic hybrid perovskite semiconductors and their application on optoelectronics.

Tae-Woo Lee is a professor in materials science and engineering at the Seoul National University, Korea. He received his Ph.D. at the Korea Advanced Institute of Science and Technology, Korea in 2002. He joined Bell Laboratories, USA as a postdoctoral researcher in 2002 and then worked at Samsung Advanced Institute of Technology as a senior member of research staff (2003-2008). He was an associate professor in materials science and engineering at the Pohang University of Science and Technology (POSTECH), Korea until August 2016. His research focuses on flexible electronics and optoelectronics using organic−inorganic hybrid perovskite semiconductors, organic semiconductors, and carbon materials for applications in displays, solid-state lighting, solar energy conversion devices, and bioinspired neuromorphic devices.

ACKNOWLEDGMENTS

This work was supported by the National Research Foundation of Korea (NRF) grant funded by the Korea government (MSIT) (2016R1A3B1908431, 2022R1C1C1008282).

REFERENCES

(1) Soneira, R. M. Display Color Gamuts: NTSC to Rec.2020. *Inf. Dispersion* **2016**, *32*, 26−31.

(2) Kim, Y.-H.; Cho, H.; Lee, T.-W. Metal Halide Perovskite Light Emitters. *Proc. Natl. Acad. Sci. U. S. A.* **2016**, *113*, 11694−11702.

(3) Kim, Y.-H.; Cho, H.; Heo, J. H.; Kim, T.-S.; Myoung, N.; Lee, C.-L.; Im, S. H.; Lee, T.-W. Multicolored Organic/Inorganic Hybrid Perovskite Light-Emitting Diodes. *Adv. Mater.* **2015**, *27*, 1248−1254.

(4) Kim, Y.-H.; Kim, J. S.; Lee, T.-W. Strategies to Improve Luminescence Efficiency of Metal-Halide Perovskites and Light-Emitting Diodes. *Adv. Mater.* **2019**, *31*, 1804595.

(5) Kim, Y.-H.; Kim, S.; Jo, S. H.; Lee, T.-W. Metal Halide Perovskites: From Crystal Formations to Light-Emitting-Diode Applications. *Small Methods* **2018**, *2*, 1800093.

(6) Chondroudis, K.; Mitzi, D. B. Electroluminescence from an Organic−Inorganic Perovskite Incorporating a Quaterthiophene Dye within Lead Halide Perovskite Layers. *Chem. Mater.* **1999**, *11*, 3028−3030.

(7) Koutselas, I.; Bampoulis, P.; Maratou, E.; Evagelinou, T.; Pagona, G.; Papavassiliou, G. C. Some Unconventional Organic−Inorganic Hybrid Low-Dimensional Semiconductors and Related Light-Emitting Devices. *J. Phys. Chem. C* **2011**, *115*, 8475−8483.

(8) Cho, H.; Jeong, S.-H.; Park, M.-H.; Kim, Y.-H.; Wolf, C.; Lee, C.-L.; Heo, J. H.; Sadhanala, A.; Myoung, N.; Yoo, S.; Im, S. H.; Friend, R. H.; Lee, T.-W. Overcoming the Electroluminescence Efficiency Limitations of Perovskite Light-Emitting Diodes. *Science* **2015**, *350*, 1222−1225.

(9) Kim, Y.-H.; Park, J.; Kim, S.; Kim, J. S.; Xu, H.; Jeong, S.-H.; Hu, B.; Lee, T.-W. Exploiting the Full Advantages of Colloidal Perovskite Nanocrystals for Large-Area Efficient Light-Emitting Diodes. *Nat. Nanotechnol.* **2022**, *17*, 590−597.

(10) Lee, T.-W.; Kim, Y.-H.; Cho, H.; Im, S.-H.; POSTECH Academy-Industry Foundation Perovskite Nanocrystalline Particles and Optoelectronic Device using Same. U.S. Patent US10193088B2, May 17, 2016.

(11) Lee, T.-W.; Kim, Y.-H.; Cho, H.; POSTECH Academy-Industry Foundation Wavelength Converting Particle, Method for Manufacturing Wavelength Converting Particle, and Light Emitting Diode Containing Wavelength Converting Particle. U.S. Patent US10424696B2, Nov. 16, 2017.

(12) Kim, Y.-H.; Wolf, C.; Kim, Y.-T.; Cho, H.; Kwon, W.; Do, S.; Sadhanala, A.; Park, C. G.; Rhee, S.-W.; Im, S. H.; Friend, R. H.; Lee, T.-W. Highly Efficient Light-Emitting Diodes of Colloidal Metal−Halide Perovskite Nanocrystals beyond Quantum Size. *ACS Nano* **2017**, *11*, 6586−6593.

(13) Jin, H.; Debroye, E.; Keshavarz, M.; Scheblykin, I. G.; Roeffaers, M. B. J.; Hofkens, J.; Steele, J. A. It's a Trap! On the Nature of Localised States and Charge Trapping in Lead Halide Perovskites. *Mater. Horizons* **2020**, *7*, 397−410.

(14) Kim, Y.-H.; Kim, S.; Kakekhani, A.; Park, J.; Park, J.; Lee, Y.-H.; Xu, H.; Nagane, S.; Wexler, R. B.; Kim, D.-H.; Jo, S. H.; Martínez-Sarti, L.; Tan, P.; Sadhanala, A.; Park, G.-S.; Kim, Y.-W.; Hu, B.; Bolink, H. J.; Yoo, S.; Friend, R. H.; Rappe, A. M.; Lee, T.-W. Comprehensive Defect Suppression in Perovskite Nanocrystals for High-Efficiency Light-Emitting Diodes. *Nat. Photonics* **2021**, *15*, 148−155.

(15) Wei, S.; Yang, Y.; Kang, X.; Wang, L.; Huang, L.; Pan, D. Room-Temperature and Gram-Scale Synthesis of $CsPbX_3$ (X = Cl, Br, I) Perovskite Nanocrystals with 50−85% Photoluminescence Quantum Yields. *Chem. Commun.* **2016**, *52*, 7265−7268.

(16) Kumar, S.; Marcato, T.; Krumeich, F.; Li, Y.-T.; Chiu, Y.-C.; Shih, C.-J. Anisotropic Nanocrystal Superlattices Overcoming Intrinsic Light Outcoupling Efficiency Limit in Perovskite Quantum Dot Light-Emitting Diodes. *Nat. Commun.* **2022**, *13*, 2106.

(17) Chiba, T.; Hayashi, Y.; Ebe, H.; Hoshi, K.; Sato, J.; Sato, S.; Pu, Y.-J.; Ohisa, S.; Kido, J. Anion-Exchange Red Perovskite Quantum Dots with Ammonium Iodine Salts for Highly Efficient Light-Emitting Devices. *Nat. Photonics* **2018**, *12*, 681−687.

(18) Dong, Y.; Wang, Y.-K.; Yuan, F.; Johnston, A.; Liu, Y.; Ma, D.; Choi, M.-J.; Chen, B.; Chekini, M.; Baek, S.-W.; Sagar, L. K.; Fan, J.; Hou, Y.; Wu, M.; Lee, S.; Sun, B.; Hoogland, S.; Quintero-Bermudez, R.; Ebe, H.; Todorovic, P.; Dinic, F.; Li, P.; Kung, H. T.; Saidaminov, M. I.; Kumacheva, E.; Spiecker, E.; Liao, L.-S.; Voznyy, O.; Lu, Z.-H.; Sargent, E. H. Bipolar-Shell Resurfacing for Blue LEDs Based on Strongly Confined Perovskite Quantum Dots. *Nat. Nanotechnol.* **2020**, *15*, 668−674.

(19) Kim, J. S.; Heo, J.-M.; Park, G.-S.; Woo, S.-J.; Cho, C.; Yun, H. J.; Kim, D.-H.; Park, J.; Lee, S.-C.; Park, S.-H.; Yoon, E.; Greenham, N. C.; Lee, T.-W. Ultra-Bright, Efficient and Stable Perovskite Light-Emitting Diodes. *Nature* **2022**, *611*, 688−694.
(20) Meloni, S.; Palermo, G.; Ashari-Astani, N.; Grätzel, M.; Rothlisberger, U. Valence and Conduction Band Tuning in Halide Perovskites for Solar Cell Applications. *J. Mater. Chem. A* **2016**, *4*, 15997−16002.
(21) Zhang, F.; Zhong, H.; Chen, C.; Wu, X.; Hu, X.; Huang, H.; Han, J.; Zou, B.; Dong, Y. Brightly-Luminescent and Color-Tunable Colloidal $CH_3NH_3PbX_3$ (X = Br, I, Cl) Quantum Dots: Potential Alternatives for Display Technology. *ACS Nano* **2015**, *9*, 4533−4542.
(22) Protesescu, L.; Yakunin, S.; Bodnarchuk, M. I.; Krieg, F.; Caputo, R.; Hendon, C. H.; Yang, R. X.; Walsh, A.; Kovalenko, M. V. Nanocrystals of Cesium Lead Halide Perovskites ($CsPbX_3$, X = Cl, Br, and I): Novel Optoelectronic Materials Showing Bright Emission with Wide Color Gamut. *Nano Lett.* **2015**, *15*, 3692−3696.
(23) Swarnkar, A.; Chulliyil, R.; Ravi, V. K.; Irfanullah, M.; Chowdhury, A.; Nag, A. Colloidal $CsPbBr_3$ Perovskite Nanocrystals: Luminescence beyond Traditional Quantum Dots. *Angew. Chemie Int. Ed.* **2015**, *54*, 15424−15428.
(24) Koscher, B. A.; Swabeck, J. K.; Bronstein, N. D.; Alivisatos, A. P. Essentially Trap-Free $CsPbBr_3$ Colloidal Nanocrystals by Postsynthetic Thiocyanate Surface Treatment. *J. Am. Chem. Soc.* **2017**, *139*, 6566−6569.
(25) Ravi, V. K.; Santra, P. K.; Joshi, N.; Chugh, J.; Singh, S. K.; Rensmo, H.; Ghosh, P.; Nag, A. Origin of the Substitution Mechanism for the Binding of Organic Ligands on the Surface of $CsPbBr_3$ Perovskite Nanocubes. *J. Phys. Chem. Lett.* **2017**, *8*, 4988−4994.
(26) Zhong, Q.; Cao, M.; Xu, Y.; Li, P.; Zhang, Y.; Hu, H.; Yang, D.; Xu, Y.; Wang, L.; Li, Y.; Zhang, X.; Zhang, Q. L-Type Ligand-Assisted Acid-Free Synthesis of $CsPbBr_3$ Nanocrystals with Near-Unity Photoluminescence Quantum Yield and High Stability. *Nano Lett.* **2019**, *19*, 4151−4157.
(27) Li, X.; Wu, Y.; Zhang, S.; Cai, B.; Gu, Y.; Song, J.; Zeng, H. $CsPbX_3$ Quantum Dots for Lighting and Displays: Room-Temperature Synthesis, Photoluminescence Superiorities, Underlying Origins and White Light-Emitting Diodes. *Adv. Funct. Mater.* **2016**, *26*, 2435−2445.
(28) Liu, P.; Chen, W.; Wang, W.; Xu, B.; Wu, D.; Hao, J.; Cao, W.; Fang, F.; Li, Y.; Zeng, Y.; Pan, R.; Chen, S.; Cao, W.; Sun, X. W.; Wang, K. Halide-Rich Synthesized Cesium Lead Bromide Perovskite Nanocrystals for Light-Emitting Diodes with Improved Performance. *Chem. Mater.* **2017**, *29*, 5168−5173.
(29) Kim, Y.-H.; Lee, G.-H.; Kim, Y.-T.; Wolf, C.; Yun, H. J.; Kwon, W.; Park, C. G.; Lee, T.-W. High Efficiency Perovskite Light-Emitting Diodes of Ligand-Engineered Colloidal Formamidinium Lead Bromide Nanoparticles. *Nano Energy* **2017**, *38*, 51−58.
(30) Li, G.; Huang, J.; Zhu, H.; Li, Y.; Tang, J. X.; Jiang, Y. Surface Ligand Engineering for Near-Unity Quantum Yield Inorganic Halide Perovskite QDs and High-Performance QLEDs. *Chem. Mater.* **2018**, *30*, 6099−6107.
(31) Lee, T.-W.; Kim, Y.-H.; Cho, H.; Im, S.-H.; POSTECH Academy-Industry Foundation. . Method for Manufacturing Perovskite Nanocrystal Particle Light Emitting Body where Organic Ligand is Substituted, Nanocrystal Particle Light Emitting Body Manufactured thereby, and Light Emitting Device using Same. U.S. Patent US20170369772A1, Dec. 28, 2017.
(32) Swarnkar, A.; Marshall, A. R.; Sanehira, E. M.; Chernomordik, B. D.; Moore, D. T.; Christians, J. A.; Chakrabarti, T.; Luther, J. M. Quantum Dot-Induced Phase Stabilization of α-$CsPbI_3$ Perovskite for High-Efficiency Photovoltaics. *Science* **2016**, *354*, 92−95.
(33) Li, J.; Xu, L.; Wang, T.; Song, J.; Chen, J.; Xue, J.; Dong, Y.; Cai, B.; Shan, Q.; Han, B.; Zeng, H. 50-Fold EQE Improvement up to 6.27% of Solution-Processed All-Inorganic Perovskite $CsPbBr_3$ QLEDs via Surface Ligand Density Control. *Adv. Mater.* **2017**, *29*, 1603885.
(34) Grisorio, R.; Di Clemente, M. E.; Fanizza, E.; Allegretta, I.; Altamura, D.; Striccoli, M.; Terzano, R.; Giannini, C.; Irimia-Vladu, M.; Suranna, G. P. Exploring the Surface Chemistry of Cesium Lead Halide Perovskite Nanocrystals. *Nanoscale* **2019**, *11*, 986−999.
(35) Hoshi, K.; Chiba, T.; Sato, J.; Hayashi, Y.; Takahashi, Y.; Ebe, H.; Ohisa, S.; Kido, J. Purification of Perovskite Quantum Dots Using Low-Dielectric-Constant Washing Solvent "Diglyme" for Highly Efficient Light-Emitting Devices. *ACS Appl. Mater. Interfaces* **2018**, *10*, 24607−24612.
(36) Chiba, T.; Hoshi, K.; Pu, Y.-J.; Takeda, Y.; Hayashi, Y.; Ohisa, S.; Kawata, S.; Kido, J. High-Efficiency Perovskite Quantum-Dot Light-Emitting Devices by Effective Washing Process and Interfacial Energy Level Alignment. *ACS Appl. Mater. Interfaces* **2017**, *9*, 18054−18060.
(37) Pan, J.; Quan, L. N.; Zhao, Y.; Peng, W.; Murali, B.; Sarmah, S. P.; Yuan, M.; Sinatra, L.; Alyami, N. M.; Liu, J.; Yassitepe, E.; Yang, Z.; Voznyy, O.; Comin, R.; Hedhili, M. N.; Mohammed, O. F.; Lu, Z. H.; Kim, D. H.; Sargent, E. H.; Bakr, O. M. Highly Efficient Perovskite-Quantum-Dot Light-Emitting Diodes by Surface Engineering. *Adv. Mater.* **2016**, *28*, 8718−8725.
(38) Bi, C.; Yao, Z.; Sun, X.; Wei, X.; Wang, J.; Tian, J. Perovskite Quantum Dots with Ultralow Trap Density by Acid Etching-Driven Ligand Exchange for High Luminance and Stable Pure-Blue Light-Emitting Diodes. *Adv. Mater.* **2021**, *33*, 2006722.
(39) Song, J.; Fang, T.; Li, J.; Xu, L.; Zhang, F.; Han, B.; Shan, Q.; Zeng, H. Organic−Inorganic Hybrid Passivation Enables Perovskite QLEDs with an EQE of 16.48%. *Adv. Mater.* **2018**, *30*, 1805409.
(40) Zhang, B.-B.; Yuan, S.; Ma, J.-P.; Zhou, Y.; Hou, J.; Chen, X.; Zheng, W.; Shen, H.; Wang, X.-C.; Sun, B.; Bakr, O. M.; Liao, L.-S.; Sun, H.-T. General Mild Reaction Creates Highly Luminescent Organic-Ligand-Lacking Halide Perovskite Nanocrystals for Efficient Light-Emitting Diodes. *J. Am. Chem. Soc.* **2019**, *141*, 15423−15432.
(41) Wang, Y.; Yuan, F.; Dong, Y.; Li, J.; Johnston, A.; Chen, B.; Saidaminov, M. I.; Zhou, C.; Zheng, X.; Hou, Y.; Bertens, K.; Ebe, H.; Ma, D.; Deng, Z.; Yuan, S.; Chen, R.; Sagar, L. K.; Liu, J.; Fan, J.; Li, P.; Li, X.; Gao, Y.; Fung, M.; Lu, Z.; Bakr, O. M.; Liao, L.; Sargent, E. H. All-Inorganic Quantum-Dot LEDs Based on a Phase-Stabilized α-$CsPbI_3$ Perovskite. *Angew. Chemie Int. Ed.* **2021**, *60*, 16164−16170.
(42) Zheng, X.; Yuan, S.; Liu, J.; Yin, J.; Yuan, F.; Shen, W.-S.; Yao, K.; Wei, M.; Zhou, C.; Song, K.; Zhang, B.-B.; Lin, Y.; Hedhili, M. N.; Wehbe, N.; Han, Y.; Sun, H.-T.; Lu, Z.-H.; Anthopoulos, T. D.; Mohammed, O. F.; Sargent, E. H.; Liao, L.-S.; Bakr, O. M. Chlorine Vacancy Passivation in Mixed Halide Perovskite Quantum Dots by Organic Pseudohalides Enables Efficient Rec. 2020 Blue Light-Emitting Diodes. *ACS Energy Lett.* **2020**, *5*, 793−798.
(43) Liu, Y.; Dong, Y.; Zhu, T.; Ma, D.; Proppe, A.; Chen, B.; Zheng, C.; Hou, Y.; Lee, S.; Sun, B.; Jung, E. H.; Yuan, F.; Wang, Y.; Sagar, L. K.; Hoogland, S.; García de Arquer, F. P.; Choi, M.-J.; Singh, K.; Kelley, S. O.; Voznyy, O.; Lu, Z.-H.; Sargent, E. H. Bright and Stable Light-Emitting Diodes Based on Perovskite Quantum Dots in Perovskite Matrix. *J. Am. Chem. Soc.* **2021**, *143*, 15606−15615.
(44) De Roo, J.; Ibáñez, M.; Geiregat, P.; Nedelcu, G.; Walravens, W.; Maes, J.; Martins, J. C.; Van Driessche, I.; Kovalenko, M. V.; Hens, Z. Highly Dynamic Ligand Binding and Light Absorption Coefficient of Cesium Lead Bromide Perovskite Nanocrystals. *ACS Nano* **2016**, *10*, 2071−2081.
(45) Lu, M.; Zhang, X.; Zhang, Y.; Guo, J.; Shen, X.; Yu, W. W.; Rogach, A. L. Simultaneous Strontium Doping and Chlorine Surface Passivation Improve Luminescence Intensity and Stability of $CsPbI_3$ Nanocrystals Enabling Efficient Light-Emitting Devices. *Adv. Mater.* **2018**, *30*, 1804691.
(46) Deng, W.; Xu, X.; Zhang, X.; Zhang, Y.; Jin, X.; Wang, L.; Lee, S.-T.; Jie, J. Organometal Halide Perovskite Quantum Dot Light-Emitting Diodes. *Adv. Funct. Mater.* **2016**, *26*, 4797−4802.
(47) Zhang, X.; Lin, H.; Huang, H.; Reckmeier, C.; Zhang, Y.; Choy, W. C. H.; Rogach, A. L. Enhancing the Brightness of Cesium Lead Halide Perovskite Nanocrystal Based Green Light-Emitting Devices through the Interface Engineering with Perfluorinated Ionomer. *Nano Lett.* **2016**, *16*, 1415−1420.

https://doi.org/10.1021/accountsmr.3c00039
Acc. Mater. Res. 2023, 4, 655−667

(48) Zhang, X.; Sun, C.; Zhang, Y.; Wu, H.; Ji, C.; Chuai, Y.; Wang, P.; Wen, S.; Zhang, C.; Yu, W. W. Bright Perovskite Nanocrystal Films for Efficient Light-Emitting Devices. *J. Phys. Chem. Lett.* **2016**, *7*, 4602−4610.
(49) Yao, Z.; Bi, C.; Liu, A.; Zhang, M.; Tian, J. High Brightness and Stability Pure-Blue Perovskite Light-Emitting Diodes Based on a Novel Structural Quantum-Dot Film. *Nano Energy* **2022**, *95*, 106974.
(50) Cao, F.; Wu, Q.; Li, W.; Wang, S.; Kong, L.; Zhang, J.; Zhang, X.; Li, H.; Hua, W.; Rogach, A. L.; Yang, X. Core/Shell ZnO/ZnS Nanoparticle Electron Transport Layers Enable Efficient All-Solution-Processed Perovskite Light-Emitting Diodes. *Small* **2023**, *19*, 2207260.
(51) Naujoks, T.; Jayabalan, R.; Kirsch, C.; Zu, F.; Mandal, M.; Wahl, J.; Waibel, M.; Opitz, A.; Koch, N.; Andrienko, D.; Scheele, M.; Brütting, W. Quantum Efficiency Enhancement of Lead-Halide Perovskite Nanocrystal LEDs by Organic Lithium Salt Treatment. *ACS Appl. Mater. Interfaces* **2022**, *14*, 28985−28996.
(52) Zhao, X.; Tan, Z.-K. Large-Area near-Infrared Perovskite Light-Emitting Diodes. *Nat. Photonics* **2020**, *14*, 215−218.
(53) Sun, C.; Jiang, Y.; Cui, M.; Qiao, L.; Wei, J.; Huang, Y.; Zhang, L.; He, T.; Li, S.; Hsu, H.-Y.; Qin, C.; Long, R.; Yuan, M. High-Performance Large-Area Quasi-2D Perovskite Light-Emitting Diodes. *Nat. Commun.* **2021**, *12*, 2207.
(54) Kong, L.; Zhang, X.; Zhang, C.; Wang, L.; Wang, S.; Cao, F.; Zhao, D.; Rogach, A. L.; Yang, X. Stability of Perovskite Light-Emitting Diodes: Existing Issues and Mitigation Strategies Related to Both Material and Device Aspects. *Adv. Mater.* **2022**, *34*, 2205217.
(55) Jiang, Y.; Sun, C.; Xu, J.; Li, S.; Cui, M.; Fu, X.; Liu, Y.; Liu, Y.; Wan, H.; Wei, K.; Zhou, T.; Zhang, W.; Yang, Y.; Yang, J.; Qin, C.; Gao, S.; Pan, J.; Liu, Y.; Hoogland, S.; Sargent, E. H.; Chen, J.; Yuan, M. Synthesis-on-Substrate of Quantum Dot Solids. *Nature* **2022**, *612*, 679−684.
(56) Zhang, C.; Wang, S.; Li, X.; Yuan, M.; Turyanska, L.; Yang, X. Core/Shell Perovskite Nanocrystals: Synthesis of Highly Efficient and Environmentally Stable $FAPbBr_3/CsPbBr_3$ for LED Applications. *Adv. Funct. Mater.* **2020**, *30*, 1910582.
(57) Zhang, C.; Chen, J.; Kong, L.; Wang, L.; Wang, S.; Chen, W.; Mao, R.; Turyanska, L.; Jia, G.; Yang, X. Core/Shell Metal Halide Perovskite Nanocrystals for Optoelectronic Applications. *Adv. Funct. Mater.* **2021**, *31*, 2100438.
(58) Woo, J. Y.; Park, M.-H.; Jeong, S.-H.; Kim, Y.-H.; Kim, B.; Lee, T.-W.; Han, T.-H. Advances in Solution-processed OLEDs and Their Prospects for Use in Displays. *Adv. Mater.* **2023**, 2207454.
(59) Lee, T.-W.; Kim, Y.-H.; Cho, H.; Im, S.-H.; POSTECH Academy-Industry Foundation. Core-Shell Structured Perovskite Particle Light-Emitter, Method of Preparing the Same and Light Emitting Device using the Same. U.S. Patent US11205757, Nov. 30, 2017.
(60) Lee, T.-W.; Kim, Y.-H.; Cho, H.; Im, S.-H.; POSTECH Academy-Industry Foundation. Perovskite Nanocrystal Particle Light-Emitter whose Content is Changed, Method of Producing the Same, and Light Emitting Element using the Same. U.S. Patent US10047284B2, Nov. 30, 2017.
(61) Heo, J.-M.; Cho, H.; Lee, S.-C.; Park, M.-H.; Kim, J. S.; Kim, H.; Park, J.; Kim, Y.-H.; Yun, H. J.; Yoon, E.; Kim, D.-H.; Ahn, S.; Kwon, S.-J.; Park, C.-Y.; Lee, T.-W. Bright Lead-Free Inorganic $CsSnBr_3$ Perovskite Light-Emitting Diodes. *ACS Energy Lett.* **2022**, *7*, 2807−2815.
(62) Yao, M.-M.; Jiang, C.-H.; Yao, J.-S.; Wang, K.-H.; Chen, C.; Yin, Y.-C.; Zhu, B.-S.; Chen, T.; Yao, H.-B. General Synthesis of Lead-Free Metal Halide Perovskite Colloidal Nanocrystals in 1-Dodecanol. *Inorg. Chem.* **2019**, *58*, 11807−11818.
(63) Fan, Q.; Biesold-McGee, G. V.; Ma, J.; Xu, Q.; Pan, S.; Peng, J.; Lin, Z. Lead-Free Halide Perovskite Nanocrystals: Crystal Structures, Synthesis, Stabilities, and Optical Properties. *Angew. Chemie Int. Ed.* **2020**, *59*, 1030−1046.
(64) Chen, H.; Fan, L.; Zhang, R.; Bao, C.; Zhao, H.; Xiang, W.; Liu, W.; Niu, G.; Guo, R.; Zhang, L.; Wang, L. High-Efficiency Formamidinium Lead Bromide Perovskite Nanocrystal-Based Light-Emitting Diodes Fabricated via a Surface Defect Self-Passivation Strategy. *Adv. Opt. Mater.* **2020**, *8*, 1901390.

https://doi.org/10.1021/accountsmr.3c00039
Acc. Mater. Res. 2023, 4, 655−667